Growth of epitaxial CdTe thin films on amorphous substrates using single crystal graphene buffer

Dibyajyoti Mohanty [a, b], Zonghuan Lu [b], Xin Sun [b, *], Yu Xiang [b, f], Lei Gao [c], Jian Shi [d], Lihua Zhang [e], Kim Kisslinger [e], Morris A. Washington [b, f], Gwo-Ching Wang [b, f], Toh-Ming Lu [b, f], Ishwara B. Bhat [a, b]

[a] Department of Electrical, Computer and Systems Engineering, Rensselaer Polytechnic Institute, Troy, NY 12180, United States
[b] Center for Materials, Devices and Integrated Systems, Rensselaer Polytechnic Institute, Troy, NY 12180, United States
[c] Corrosion and Protection Center, Key Laboratory for Environmental Fracture (MOE), University of Science and Technology Beijing, Beijing 100083, China
[d] Department of Materials Science and Engineering, Rensselaer Polytechnic Institute, Troy, NY 12180, United States
[e] Brookhaven National Laboratory, Center for Functional Nanomaterials, P.O. Box 5000, Upton, NY 11973, United States
[f] Department of Physics, Applied Physics and Astronomy, Rensselaer Polytechnic Institute, Troy, NY 12180, United States

ARTICLE INFO

ABSTRACT

Traditionally, a high-quality CdTe film can only be grown on a single crystal substrate with a small lattice mismatch. Herein, we report the epitaxy of CdTe films on monolayer single crystal graphene buffered amorphous $SiO_2/Si(100)$ substrates, despite a 86% lattice mismatch between CdTe(111) and graphene. X-ray pole figure, electron backscatter diffraction mapping and transmission electron microscopy all confirm that the epitaxial CdTe films are composed of two domains: the primary and the $\Sigma3$ twin. The crystal quality of films is shown to improve as the post-deposition annealing temperature increases. However, the rotational misalignment in CdTe remains large even after annealing. Through density functional theory calculations on the charge transfer distribution at the interface of CdTe and graphene, it is found that the interface is dominated by the weak van der Waals interaction, which explains the large spread of in-plane orientation in CdTe films. Furthermore, the rotational misalignment in graphene itself is also confirmed to produce the large in-plane orientation spread in CdTe films. Although imperfect in epitaxy quality, this work demonstrates that monolayer single crystal graphene can buffer amorphous substrates for growing epitaxial films, and hence hints an opportunity for developing advanced thin film devices using graphene as a template.

© 2018 Elsevier Ltd. All rights reserved.

1. Introduction

CdTe, a II-VI compound semiconductor, is an integral component of many important optoelectronic devices. Quality CdTe films are typically grown on single crystal substrates using heteroepitaxy mechanism, bearing on the desired lattice matching between films and substrates. Due to this restriction, limited choices of substrates can be utilized. Moreover, the strong chemical bonding at interfaces, especially in the case of large mismatched interfaces, could produce interfacial strain which propagates into the growing film. Beyond a critical film thickness, defects, such as dislocations, would be generated and thread into films, leaving deteriorated film

quality.

Recently, there has been increasing interest in growing epitaxial films on substrates through van der Waals (vdW) interactions. In vdW epitaxy (vdWE) the requirement of lattice matching may be relieved since chemical bonding is not required at the interface [1]. As a result, the strain could be relaxed at the interface and the film becomes incommensurate [2]. There are many reports of vdWE of two-dimensional (2D) layered overlayers on 2D layered substrates [3−9]. On the other hand, the epitaxial growth of 3D semiconductor overlayers on 2D layered substrates, such as graphene, has been known challenging and less studied [10−14].

Herein, using a two-step metalorganic chemical vapor deposition (MOCVD) method, we demonstrate the epitaxial growth of CdTe(111) films on monolayer single crystal graphene buffered amorphous $SiO_2/Si(100)$ substrates. In spite of a 86% (100%*(4.58-2.46) Å/2.46 Å) in-plane lattice mismatch between CdTe(111) and

graphene, the epitaxial alignment of CdTe(111) (containing the primary and its twin domain) can be clearly observed. The single crystalline nature of CdTe films, composed of twin domains though, is in contrast to that in our previous study where multiple rotational domains in CdTe films were obtained on polycrystalline graphene [15]. Using density functional theory (DFT), we calculate the charge transfer distribution and interfacial interaction between CdTe(111) and graphene. The calculations reveal that the van der Waals force dominates at the interface.

Albeit the interaction coming out of graphene substrate is weak, the fact that graphene can promote epitaxial growth of 3D semiconductor films proves the sufficient strength of monolayer graphene, in spite of only one atomic layer thick, for ordering the atomic arrangement of "heavy" 3D materials. Also, the finding in this work brings second thoughts to the claim of total transparency of monolayer graphene. If truly totally transparent in graphene, the CdTe film growth would act as if on amorphous substrates and show no sign of epitaxy. For the technology point of view, the demonstration of epitaxy of traditional semiconductor thin films on graphene opens new avenue to novel optoelectronic devices. For example, single crystal CdTe is a desirable substrate for high-quality epitaxial $Hg_{1-x}Cd_xTe$ thin film used as infrared detectors [16]. The conventional strategy for this application is to use a heterojunction such as $Hg_{1-x}Cd_xTe/CdTe/GaAs$ or $Hg_{1-x}Cd_xTe/CdTe/Si$. If graphene is chosen to replace GaAs or Si, the biggest appeal of this $Hg_{1-x}Cd_xTe/CdTe/graphene$ heterojunction is that the $Hg_{1-x}Cd_xTe/CdTe$ layer can be transferred to the readout electronic wafer without the substrate, which thus significantly reduces undesired absorption of radiation by the GaAs or Si substrate.

2. Results and discussion

The single crystal graphene used in this work was synthesized on epitaxial Cu(111) films using a low pressure CVD method. The epitaxial Cu(111) films were firstly prepared by sputtering on *c*-sapphire and subsequently used as the catalyst for graphene growth at 1020 °C. CH_4 (10 standard cubic centimeter per minute or sccm) and H_2 (35 sccm) in 200 sccm Ar carrier gas were used for the CVD reaction at a chamber pressure of ~50 Torr. The graphene was transferred to SiO$_2$/Si(100) substrates using a standard wet transfer process [17]. Details regarding graphene growth and transfer can be

found in the supplementary data and elsewhere [18]. Fig. 1(a) shows an optical image of the graphene transferred onto a SiO$_2$/Si(100) substrate. The uniform contrast suggests a large-scale homogeneity. The overlaying curve in Fig. 1(a) is a representative Raman spectrum of the graphene. The D, G and 2D peaks are observed around 1340, 1586 and 2674 cm^{-1}, respectively. The intensity ratio of 2D to G in peak area, ~3.8, implies the monolayer nature of graphene [19,20]. The CdTe film, 750 nm thick, was grown on the graphene/SiO$_2$/Si(100) substrate using a two-step MOCVD process. A ~10 nm CdTe layer was firstly grown at 300 °C substrate temperature for enhanced nucleation, followed by film deposition at 450 °C substrate temperature. The post-deposition annealing was conducted in H$_2$ at 450, 550 and 650 °C for 30, 20 and 20 min, respectively. Details of the film processing is described in the supplementary data. Figs. 1(b−d) show the scanning electron microscopy (SEM) images of the CdTe films on graphene after annealing at 450, 550 and 650 °C, respectively. The morphology of the as-grown CdTe film is similar to that of the 450 °C annealed film and hence is not shown. As the annealing temperature increases, it is seen that the lateral feature sizes increase from sub-μm to several μm. These sizes are consistent with the electron backscatter diffraction (EBSD) data to be presented later. It should be noted that some areas in Fig. 2(d) have dark contrast, indicative of film evaporation at this temperature. Fig. 2(e) shows a room temperature Raman spectrum measured from the CdTe film after annealing at 550 °C. The spectrum can be fitted by four peaks, namely, E mode of Te at 91 cm^{-1}, A_1 mode of Te 120 cm^{-1}, E mode of Te or TO mode of CdTe at 139 cm^{-1} and LO mode of CdTe at 161 cm^{-1} [21,22]. Raman spectra of films annealed at the other two conditions are similar. See Table S1. In general, peak positions and full-width-at-the-half-maximums (FWHMs) are comparable to those in the literature and suggest local order and stoichiometry of the CdTe films.

Fig. 1(f) shows x-ray diffraction (XRD) θ-2θ scan of the CdTe film after annealing at 550 °C. The out-of-plane orientation of CdTe is clearly along the (111) direction. The interlayer spacing (d_{111}) is determined to be 3.74 Å, close to the d_{111} of bulk CdTe. Similar results can be found for films annealed at 450 and 650 °C, shown in Figs. S1(a) and (b). For in-plane orientation, Fig. 1(g) shows (111) azimuthal scan (2θ = 23.79° and χ = 70.5°) of the sample in Fig. 1(f). A six-fold symmetry is observed. Theoretically, the (111) azimuthal scan of cubic CdTe should give rise to a three-fold symmetry. By
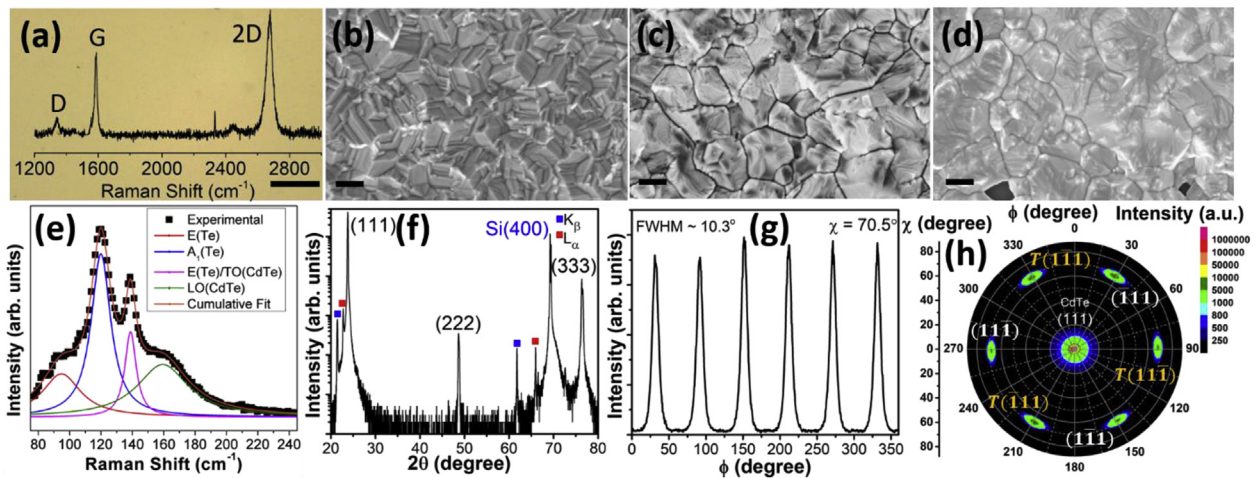
Fig. 1. (a) Optical image of the monolayer graphene on SiO$_2$/Si(100). Scale bar: 15 μm. Overlaid: Raman spectrum of the monolayer graphene. (b−d) SEM images of CdTe films on graphene after 450, 550 and 650 °C annealing, respectively. Scale bar: 500 nm. (e) Raman spectrum and its deconvoluted fitting curves of the CdTe film on graphene after annealing at 550 °C. (f) XRD θ-2θ scan of the CdTe film on graphene after annealing at 550 °C. (g) X-ray azimuthal scan of CdTe(111) of the film in (f). (h) X-ray pole figure of CdTe {111} of the film in (f). The pole figure has six visible poles at χ ~70° in addition to the central pole. *T* represents twin. (A colour version of this figure can be viewed online.)
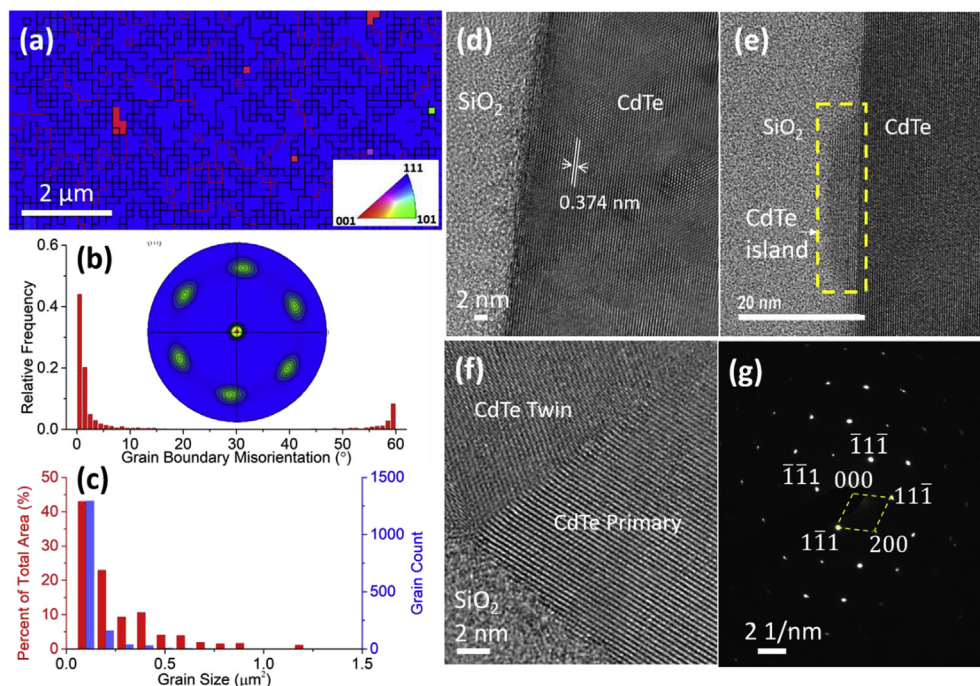
Fig. 2. (a) EBSD crystallographic orientation map using IPF-Z component for the CdTe film on graphene after 550 °C annealing. Grain boundaries shown in the maps with red curves indicating twin boundaries and black curves indicating other grain boundaries. (b) Histogram of grain boundary misorientation distribution based on the map in (a). Inset: EBSD pole figure of CdTe {111}. (c) Histogram of grain size distribution (in area) based on the map in (a). The left Y axis (red) representing the Percentage of Total Area occupied by grains with the specified grain size, and the right Y axis (blue) representing the Count of grains with the specified grain size. (d) High resolution TEM image of the as-grown CdTe film on graphene/SiO₂/Si(100). Film thickness: 350 ± 50 nm. (e) A representative CdTe nanoisland protruding into SiO₂ layer highlighted by dashed yellow lines. (f) High resolution TEM image showing a twin boundary between a primary CdTe grain and a twin grain. (g) Selected area electron diffraction pattern from the CdTe film with the Miller indices and unit mesh labeled. Zone axis: [011]. (A colour version of this figure can be viewed online.)

observing two sets of three-fold symmetries in Fig. 1(g), we conclude that in this film there are two (111) domains that are 60° in-plane twin to each other. The twinning effect will be verified in real space by a high-resolution transmission electron microscopy (TEM) image later. The average FWHM of six peaks in Fig. 1(g) is around 10.3°, meaning the dispersion of in-plane orientation is relatively large. For films annealed at 450 and 650 °C, the six-fold symmetry in (111) azimuthal scans is found, too (Figs. S1(c) and (d)). The FWHM of 650 °C annealed film is similar to that of 550 °C annealed. However, the FWHM of 450 °C annealed film is almost twice larger, suggesting that the higher temperature anneal is useful to improve the in-plane orientation. X-ray pole figure of CdTe {111}, shown in Fig. 1(h), reveals the texture of the CdTe film annealed at 550 °C. In line with θ-2θ and azimuthal scans, an intense CdTe (111) pole at the center ($\chi = 0°$) indicates the out-of-plane orientation, and six poles at χ ~70.5° separated by 60° in azimuthal angle indicate two in-plane domains. The label *T* represents twin poles. Except for six poles identified above, there is no additional pole in Fig. 1(h), different from our previous study in which a total of 12 poles, indicative of four in-plane domains, were observed at χ ~70.5° for a similar CdTe film grown on poly-crystalline graphene [15]. This direct comparison suggests that the crystallinity of graphene (single crystal versus poly-crystal) strongly affects the domain structure of films grown atop.

To further examine the crystallographic orientation and the grain distribution, EBSD inverse pole figure (IPF) Z mapping of the CdTe film after annealing at 550 °C is shown in Fig. 2(a). The mapping shows a uniform [111] out-of-plane orientation across the scan area and two types of in-plane boundaries. The red curves represent twin boundaries (Σ3 coincidence site lattice boundary), and the black curves represent other grain boundaries. Figure 2(b) shows the histogram of grain boundary misorientation distribution.

There is a high total frequency (~80%) of orientation located at 0–2° and 58–60°, which is a measure of the abundant twin boundaries. There also exist low frequencies (~20%) of random grain boundary misoriented from ~3° to ~57°. Inset of Fig. 2(b) shows the corresponding EBSD pole figures of CdTe {111} with six symmetrical poles, consistent with the x-ray pole figure shown in Fig. 1(h). The EBSD grain (twin grains mostly) size distribution (in area) is shown in Fig. 2(c). For this 550 °C annealed film, the majority of grains are characterized with a size less than 1 μm ($= \sqrt{1\ μm^2}$). In summary, the EBSD data concludes that the film is composed of small grains, although collectively all grains are preferably aligned in the same out-of-plane and in-plane orientations. Fig. S2 displays the EBSD data of 450 and 650 °C annealed films. The temperature dependent trend is found as the following: with increasing temperature, the percentage of randomly misoriented grains decreases and the grain size increases.

A CdTe film on graphene/SiO₂/Si(100) with a reduced thickness (350 ± 50 nm) was prepared for TEM study. The growth condition for this film was the same as that for abovementioned samples, except this film was not annealed after deposition. Fig. 2(d) shows a high resolution TEM image of this sample. The SiO₂ shows the typical feature of an amorphous phase in contrast to the highly ordered CdTe film. From the line scan perpendicular to the interface, the average interlayer spacing of CdTe film is determined to be 3.74 Å, consistent with the CdTe bulk value of $d_{111} = 3.74$ Å ($= 6.48/\sqrt{3}$ Å). This d_{111} value also supports the conclusion from the XRD and EBSD measurements that the out-of-plane direction of the CdTe film is the [111]. The surface of SiO₂ is supposed to be smooth, but, when graphene is transferred on it, the graphene could produce wrinkles and folding. This explains why the interface between CdTe and SiO₂ is not atomically smooth like the original SiO₂ surface. The roughness of interface is about one to two interlayer d_{111}

of CdTe. Consequently, it is challenging to identify the exact location of graphene. If the supporting substrate for graphene is a single crystal, for example, when graphene is grown on single crystal Ru(0001) and then hosts subsequent growth of Ru clusters, both sides of graphene have the same and regular lattice. In that case, the graphene can be readily identified [23]. Unfortunately, it is not the case for this study. Nevertheless, it should be emphasized that graphene is expected to exist at the interface even though TEM imaging does not see it. Because, if there is no graphene, the CdTe film cannot grow in epitaxial format on the unbuffered amorphous SiO$_2$ surface. As clearly demonstrated in the XRD and EBSD pole figures, our CdTe films have preferred in-plane orientations, which must be the outcome of single crystal graphene buffering.

Fig. 2(e) shows that at some sites CdTe nanoislands protrude from the CdTe side to the SiO$_2$ side. The nanoisland length parallel to the interface ranges from 5 to 20 nm and the thickness ranges from 5 to 10 nm. Most nanoislands have the (111) out-of-plane orientation. Since the graphene could not be identified, the cause of this protrusion is not clear. But it is speculated that the growth of CdTe nanoislands starts from the defected region of graphene, most likely in the format of multiatom vacancy [24]. Fig. 2(f) is a high-resolution image of the CdTe film showing part of a primary CdTe grain, part of a twin grain and a twin boundary between them. Selected area electron diffraction pattern of the CdTe grain, shown in Fig. 2(g), confirms that the CdTe film is single-crystalline-like epitaxial film. The unit mesh is highlighted in yellow dashed lines, and the zone axis is determined to be [011]. When the diffraction pattern is collected from the primary and twin region, the TEM pattern has the typical twin spots on both sides of twin axis [25,26].

Although preferred in-plane orientation of CdTe films on graphene is experimentally confirmed in this study, it is acknowledged that the epitaxy quality is poor, evident from the large dispersion of in-plane orientation and the small grain size in films. This observation is in sharp contrast to the epitaxy quality of CdTe films grown by MOCVD on mica that is also a 2D layered substrate [27]. In our previous work on the case of CdTe on mica, the dispersion of in-plane orientation is smaller than 0.38° and the grain size is larger than 250 μm. DFT calculations reveal that chemical interaction and vdW interaction contribute ~80% and ~20% to the total interface energy, respectively, at the interface of CdTe and mica. The calculations reshape the understanding of mica as a pure vdW material, and we attribute the high quality of CdTe films on mica to the large chemical contribution at the interface. Herein, we seek to expand our understanding of CdTe-graphene interface using a similar DFT methodology.

According to our previous analysis, the epitaxial alignment between CdTe and graphene most likely has the following relationship: out-of-plane, CdTe(111) ∥ graphene basal plane and in-plane, CdTe [$\overline{11}2$] ∥ graphene [10] [15]. We thus use this orientational configuration to set up the DFT model for the present study. The unit cell of graphene is defined as a = b = 4.26 Å and α = 60° and the unit cell of CdTe(111) is defined as a = b = 4.58 Å and α = 60°, shown by the red dashed parallelograms in Fig. 3(a). The supercell is selected as three-layer of 9 × 9 CdTe sitting on monolayer of 10 × 10 graphene, with about 3% compressive strain imposed on graphene. See Fig. 3(b). The selection of this model is mainly based on following criteria: reducing the macro strain on graphene and meanwhile keeping the scale of supercell within the limit of DFT calculation. The monolayer graphene (including 600 C atoms) is fixed during the relaxation of three-layer of CdTe (including 243 Cd atoms and 243 Te atoms). CdTe lattices are allowed to relax until the forces on all relaxed atoms are less than 0.05 eV/Å. Although a relative large strain is imposed on graphene, the characteristics of the interface between graphene and CdTe could still be probed

qualitatively. Fig. 3(c) shows the top-view of the CdTe (bottom layer shown only) on graphene after relaxation. Fig. 3(d) presents the corresponding charge transfer distribution between CdTe and graphene, which reflects a relative weak interfacial interaction between them. Next, the characteristics of the interfacial interactions between CdTe and graphene are further investigated by estimating the contribution of vdW interaction [28]. We first calculate the interfacial interaction including the nonlocal vdW interactions with the optB86b-vdW functional. Then, utilizing the same atomic structure, we calculate the interfacial interaction between CdTe and graphene with only the plain Perdew-Burke-Ernzerhof functional. The former interfacial interaction including vdW interaction is found to be −26.3 meV/Å^2, while the latter one without vdW interaction is 1.0 meV/Å^2. The positive value indicates the stabilizations of the interfacial structure, and the interlayer distance totally arises from the contribution of vdW interaction. Therefore, the calculation indicates that graphene, unlike mica, can be declared as a vdW dominated material when used as a substrate to grow CdTe. This result is consistent with that reported by Xie et al. [29]. Using a similar charge transfer study at the interface, they also found that the bond strength at the interface of CdTe-NbSe$_2$ is five times as large as that of the vdW interaction between CdTe-graphene. Note NbSe$_2$ is also a 2D material. Furthermore, a typical measure of the interaction strength between graphene and a material is the separation between them. Previous studies show that a separation distance around ~2.1 Å between graphene-material usually leads to a strong interaction at the interface, and the interaction strength diminishes as the separation increases and eventually minimizes at ~3.3 Å, the vdW gap in graphite [30]. In the present DFT study, the relaxed distance between CdTe and graphene is 2.93 Å after a geometry optimization. We speculate that this distance is closer to the end for weak interaction strength, which is one of reasons that the interface between CdTe and graphene is weak. In summary, the interface energy between CdTe and graphene is mainly from the vdW interaction according to the DFT calculation, even though the CdTe is not a vdW material. We suspect that such a vdW interface interaction is too weak to fully order and register the domain alignment in the CdTe film. As a consequence, a large spread of the in-plane orientation is formed in the CdTe film.

In addition to the weak interface interaction, the rotational misalignment of graphene itself can also lead to the in-plane rotational misalignment of CdTe, which is a straightforward passing effect from a substrate to an overlayer. The misalignment in graphene can be categorized in two types: transfer-induced and deposition-induced. We first consider the one post transfer to SiO$_2$/Si(100), prior to CdTe deposition. To this end, a 2D reciprocal space mapping (RSM) method was previously developed based on reflection high-energy electron diffraction (RHEED) and is referred to herein to illustrate the rotational misalignment in graphene [18]. Fig. 4(a) shows a selected RHEED pattern of monolayer graphene as-grown on Cu(111). Three bright streaks in Fig. 4(a) correspond to (00), ($\overline{2}1$) and (21) diffraction spots of graphene in the reciprocal space. To construct the RSM within the first Brillouin zone of graphene, a series of RHEED patterns were collected as the graphene was rotated azimuthally. Note, if the graphene is a single crystal, diffraction streaks can only be formed at certain azimuthal angles (Φ). In each RHEED pattern, the intensity profile along the yellow dashed line in Fig. 4(a) is extracted. All intensity profiles are then plotted as a function of Φ and a function of distance from the (00) spot to construct the RSM. Fig. 4(b) shows the RSM of the monolayer graphene as-grown on Cu(111). There are six distinct and symmetrical spots at a distance of 5.1 Å^{-1} from the center, corresponding to (21), (12), ($\overline{1}1$), ($\overline{2}1$), ($\overline{12}$) and (1$\overline{1}$) diffraction spots of graphene. The six-fold symmetry confirms that the graphene is a
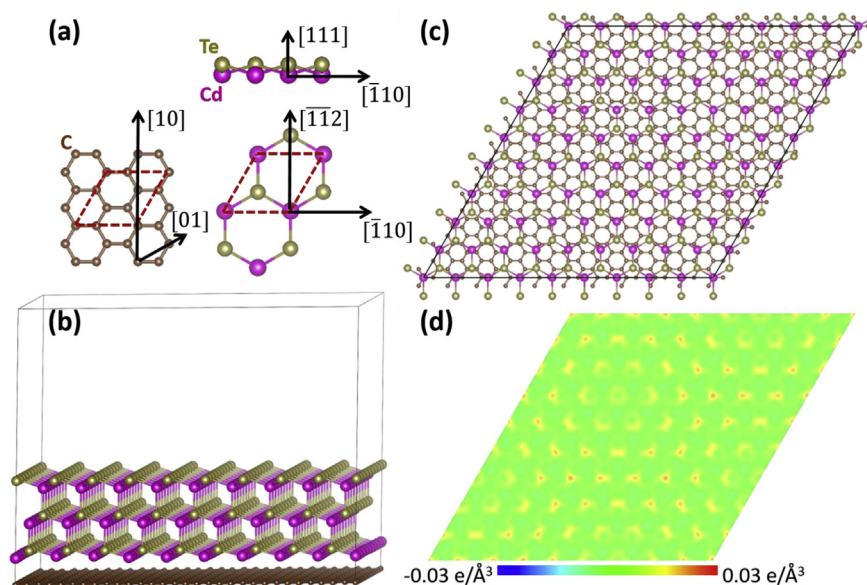
Fig. 3. DFT calculation of the interfacial interaction between CdTe(111) and monolayer graphene. (a) Alignment relationship between CdTe(111) and graphene used for the DFT calculation. Bottom: top view of CdTe(111) and graphene; red dashed parallelograms representing the definition of unit cell. Top: side view of CdTe(111). (b) Prospective view of the supercell: three-layer CdTe(111) on monolayer graphene. The size of supercell: 9x9 CdTe(111) on 10x10 graphene. (c) Top view of relaxed CdTe(111) on graphene. Only the bottom layer of CdTe(111) shown. (d) The charge transfer distribution between graphene and the bottom layer of CdTe(111). (A colour version of this figure can be viewed online.)
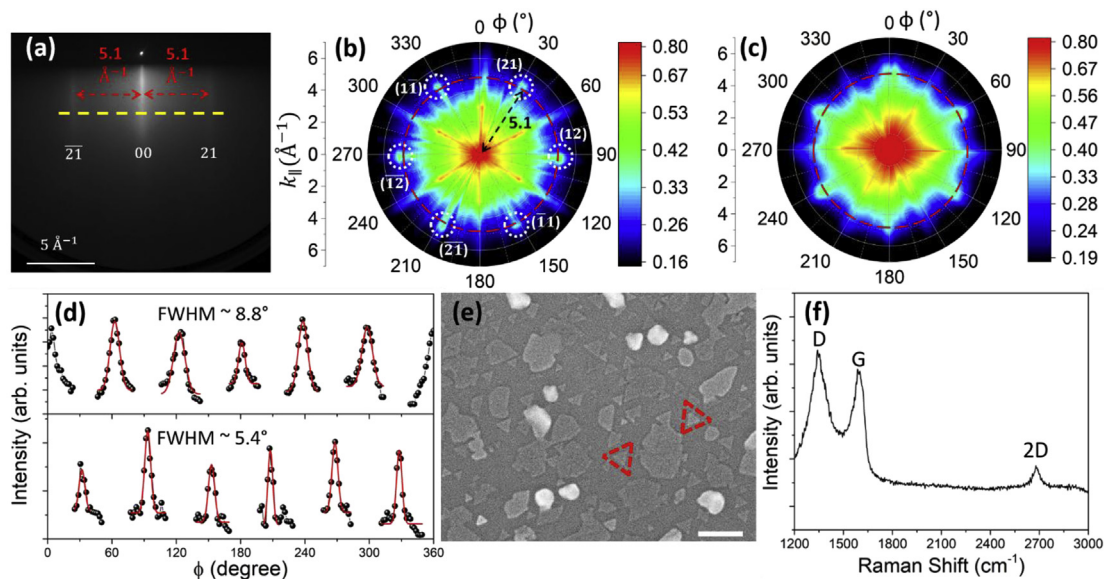
Fig. 4. (a) A RHEED pattern of monolayer graphene as-grown on Cu(111). (b) 2D RSM of monolayer graphene as-grown on Cu(111) based on a series of RHEED patterns similar to the one shown in (a). (c) 2D RSM of monolayer graphene transferred to $SiO_2/Si(100)$ using the same method as in (b). (d) Azimuthal scans along the red dashed circles (5.1 $Å^{-1}$ away from the center) shown in (b) and (c). The bottom plot is for the as grown graphene on Cu(111) in (b) and the top plot is for the transferred graphene on SiO_2 in (c). (e) SEM image of CdTe on graphene/SiO_2/Si(100) after the nucleation stage of MOCVD growth. Scale bar: 100 nm. (f) Raman spectrum of the CdTe film on graphene/SiO_2/Si(100) sample in (e). (a−c) Adapted with permission [18]. Copyright 2017, American Chemical Society. (A colour version of this figure can be viewed online.)

single domain. Similarly, Fig. 4(c) shows the RSM of monolayer graphene transferred to SiO_2/Si(100). Despite the indication of a single domain, the broadening of diffraction spots is clearly seen for the transferred graphene. The spots in Figs. 4(b) and (c) are compared by drawing the azimuthal scans at a distance of 5.1 $Å^{-1}$ from the center (red dashed circles in Figs. 4(b) and (c)) and analyzing the FWHM. Fig. 4(d) bottom panel shows that the FWHM of diffraction spots is ~5.4° for the as-grown graphene and increases to ~8.8° for the transferred graphene shown in Fig. 4(d) top panel. Apparently, the structural integrity of graphene experiences

degradation during the wet transfer process, and we should expect the existence of rotational misalignment in graphene even before the deposition of CdTe. Note, the FWHM comparison in Fig. 4(d) is only a qualitative argument and the FWHM in Fig. 4(d) cannot be compared quantitatively to the counterpart in Fig. 1(g), since different systems (XRD versus RHEED) have different instrument responses [31].

Next, we consider the rotational misalignment of graphene induced by the CdTe deposition. Fig. 4(e) shows the SEM image of CdTe on graphene/SiO_2/Si(100) at the nucleation stage of the two-

step MOCVD growth. CdTe nanoislands, mostly in triangular shape, are observed to align along two directions (60° twin to each other), labeled by the red dashed triangles in Fig. 4(e). The alignment confirms the nature of epitaxy growth followed by the nucleation stage. Fig. 4(f) shows the Raman spectrum of graphene for this particular sample at the nucleation stage. Compared to the Raman spectrum in Fig. 1(a), the significant bumping up and merging of D and G peaks in Fig. 4(f) suggests a severe disordering in graphene [32]. It is therefore concluded that the nucleation of CdTe on graphene is accompanied by a structural alteration in graphene, which would translate into the dispersion of film's orientation as the depositoin continues beyond the nucleation stage.

3. Conclusions

In summary, we present the analysis of MOCVD grown epitaxial CdTe films on monolayer single crystal graphene buffered amorphous $SiO_2/Si(100)$ substrates. XRD shows that the CdTe films have the (111) out-of-plane orientation. X-ray azimuthal scan, x-ray pole figure and EBSD pole figure show that the CdTe films contain two in-plane domains: the primary and the twin. TEM investigation further confirms the single-crystalline characteristics of these CdTe films on graphene and the existence of twin domains in CdTe films. Post-deposition annealing study shows that the higher annealing temperature, 550 °C or higher, the better film quality in terms of in-plane orientation. In general, however, the dispersion of in-plane orientation in all CdTe films is large. DFT calculations suggest that the interface energy between CdTe and graphene is dominated by vdW interaction, although CdTe is not a vdW material. The weak nature of interface energy is believed to be the main cause for the observed large in-plane dispersion in CdTe films. In addition, the rotational misalignment in graphene, including transferred-induced and deposition-induced, may also be responsible for the spread of in-plane alignment in the CdTe films. Nevertheless, our results demonstrate that epitaxial films of semiconductors can be achieved on amorphous substrates through a buffer of single crystal graphene, which sheds light on the pursuit of advanced optoelectronics.

Appendix A. Supplementary data

Supplementary data to this article can be found online at https://doi.org/10.1016/j.carbon.2018.12.094.

References

[1] A. Koma, Van der Waals epitaxy—a new epitaxial growth method for a highly lattice-mismatched system, Thin Solid Films 216 (1) (1992) 72—76.

[2] M.I. Bakti Utama, et al., Recent developments and future directions in the growth of nanostructures by van der Waals epitaxy, Nanoscale 5 (9) (2013) 3570—3588.

[3] A.K. Geim, I.V. Grigorieva, Van der Waals heterostructures, Nature 499 (7459) (2013) 419—425.

[4] T. Björkman, et al., van der Waals bonding in layered compounds from advanced density-functional first-principles calculations, Phys. Rev. Lett. 108 (23) (2012) 235502.

[5] K.K. Leung, et al., Theoretical and experimental investigations on the growth of SnS van der Waals epitaxies on graphene buffer layer, Cryst. Growth Des. 13 (11) (2013) 4755—4759.

[6] J.E. Boschker, et al., Coincident-site lattice matching during van der Waals epitaxy, Sci. Rep. 5 (2015) 18079.

[7] B. Li, et al., Strain in epitaxial Bi2Se3 grown on GaN and graphene substrates: a reflection high-energy electron diffraction study, Appl. Phys. Lett. 107 (8) (2015), 081604.

[8] A. Azizi, et al., Freestanding van der Waals heterostructures of graphene and transition metal dichalcogenides, ACS Nano 9 (5) (2015) 4882—4890.

[9] H. Ago, et al., Controlled van der Waals epitaxy of monolayer MoS2 triangular domains on graphene, ACS Appl. Mater. Interfaces 7 (9) (2015) 5265—5273.

[10] Y. Alaskar, et al., Towards van der Waals epitaxial growth of GaAs on Si using a graphene buffer layer, Adv. Funct. Mater. 24 (42) (2014) 6629—6638.

[11] J. Kim, et al., Principle of direct van der Waals epitaxy of single-crystalline films on epitaxial graphene, Nat. Commun. 5 (2014) 4836.

[12] Y. Jung, et al., Growth of CdTe thin films on graphene by close-spaced sublimation method, Appl. Phys. Lett. 103 (23) (2013) 231910.

[13] G. Yang, D. Kim, J. Kim, Self-aligned growth of CdTe photodetectors using a graphene seed layer, Optic Express 23 (19) (2015) A1081—A1086.

[14] X. Sun, et al., van der Waals epitaxy of CdS thin films on single-crystalline graphene, Appl. Phys. Lett. 110 (15) (2017) 153104.

[15] D. Mohanty, et al., van der Waals epitaxy of CdTe thin film on graphene, Appl. Phys. Lett. 109 (14) (2016) 143109.

[16] W. Lei, J. Antoszewski, L. Faraone, Progress, challenges, and opportunities for HgCdTe infrared materials and detectors, Appl. Phys. Rev. 2 (4) (2015), 041303.

[17] X. Li, et al., Large-area synthesis of high-quality and uniform graphene films on copper foils, Science 324 (5932) (2009) 1312—1314.

[18] Z. Lu, et al., Revealing the crystalline integrity of wafer-scale graphene on SiO2/Si: an azimuthal RHEED approach, ACS Appl. Mater. Interfaces 9 (27) (2017) 23081—23091.

[19] D. Graf, et al., Spatially resolved Raman spectroscopy of single- and few-layer graphene, Nano Lett. 7 (2) (2007) 238—242.

[20] A.C. Ferrari, et al., Raman spectrum of graphene and graphene layers, Phys. Rev. Lett. 97 (18) (2006) 187401.

[21] P.M. Amirtharaj, F.H. Pollak, Raman scattering study of the properties and removal of excess Te on CdTe surfaces, Appl. Phys. Lett. 45 (7) (1984) 789—791.

[22] S.S. Islam, et al., Forbidden one-Lo-phonon resonant Raman scattering and multiphonon scattering in pure CdTe crystals, Phys. Rev. B 46 (8) (1992) 4982—4985.

[23] E. Sutter, et al., Arrays of Ru nanoclusters with narrow size distribution templated by monolayer graphene on Ru, Surf. Sci. 605 (17) (2011) 1676—1684.

[24] Z.Y. Al Balushi, et al., Two-dimensional gallium nitride realized via graphene encapsulation, Nat. Mater. 15 (2016) 1166.

[25] G.C. Wang, et al., Orientational domains in metalorganic chemical vapor deposited CdTe(111) film on cube-textured Ni, Thin Solid Films 531 (2013) 217—221.

[26] Y.B. Yang, et al., Surface and interface of epitaxial CdTe film on CdS buffered van der Waals mica substrate, Appl. Surf. Sci. 413 (2017) 219—232.

[27] D. Mohanty, et al., Metalorganic vapor phase epitaxy of large size CdTe grains on mica through chemical and van der Waals interactions, Physical Review Materials 2 (11) (2018) 113402.

[28] A.N. Rudenko, et al., Graphene adhesion on mica: role of surface morphology, Phys. Rev. B 83 (4) (2011), 045409.

[29] W. Xie, et al., Enhanced van der Waals epitaxy via electron transfer enabled interfacial dative bond formation, Physical Review Materials 1 (6) (2017), 063402.

[30] A. Dahal, M. Batzill, Graphene—nickel interfaces: a review, Nanoscale 6 (5) (2014) 2548—2562.

[31] G.-C. Wang, T.-M. Lu, Instrumentation for RHEED Pole figure, in: G.-C. Wang, T.-M. Lu (Eds.), RHEED Transmission Mode and Pole Figures: Thin Film and Nanostructure Texture Analysis, Springer New York, New York, NY, 2014, pp. 107—131.

[32] Y. Wang, D.C. Alsmeyer, R.L. McCreery, Raman spectroscopy of carbon materials: structural basis of observed spectra, Chem. Mater. 2 (5) (1990) 557—563.